Article:
Assaf, E, Sheps, L, Whalley, L orcid.org/0000-0002-4486-9029 et al. (4 more authors) (2017) The Reaction between CH_3O_2 and OH Radicals: Product Yields and Atmospheric Implications. Environmental Science & Technology, 51 (4). pp. 2170-2177. ISSN 0013-936X

https://doi.org/10.1021/acs.est.6b06265

The Reaction between CH_3O_2 and OH Radicals: Product Yields and Atmospheric Implications

Emmanuel Assaf[1], Leonid Sheps[2], Lisa Whalley[3,4], Dwayne Heard[3,4], Alexandre Tomas[5], Coralie Schoemaecker[1], Christa Fittschen[1,*]

[1] Université Lille, CNRS, UMR 8522 - PC2A - Physicochimie des Processus de Combustion et de l'Atmosphère, F-59000 Lille, France

[2] Combustion Research Facility, Sandia National Laboratories, 7011 East Ave., Livermore, California 94551 USA

[3] School of Chemistry, University of Leeds, Woodhouse Lane, Leeds, LS2 9JT, UK

[4] National Centre for Atmospheric Chemistry, University of Leeds, Woodhouse Lane, Leeds, LS2 9JT, UK

[5] Mines Douai, Département Sciences de l'Atmosphère et Génie de l'Environnement (SAGE), F-59508 Douai, France

*Corresponding author: Christa Fittschen
Phone: +33 3 20 33 72 66, Fax: +33 3 20 43 69 77
e-mail: christa.fittschen@univ-lille1.fr

Revised Manuscript

Submitted to

Environmental Science & Technology

Abstract

The reaction between CH_3O_2 and OH radicals has been shown to be fast and to play an appreciable role for the removal of CH_3O_2 radials in remote environments such as the marine boundary layer. Two different experimental techniques have been used here to determine the products of this reaction. The HO_2 yield has been obtained from simultaneous time-resolved measurements of the absolute concentration of CH_3O_2, OH and HO_2 radicals by cw-CRDS. The possible formation of a Criegee intermediate has been measured by broadband cavity enhanced UV absorption. A yield of ϕ_{HO_2}= (0.8±0.2) and an upper limit for $\phi_{Criegee}$= 0.05 has been determined for this reaction, suggesting a minor yield of methanol or stabilized trioxide as a product. The impact of this reaction on the composition of the remote marine boundary layer has been determined by implementing these findings into a box model utilizing the Master Chemical Mechanism v3.2, and constraining the model for conditions found at the Cape Verde Atmospheric Observatory in the remote tropical Atlantic Ocean. Inclusion of the CH_3O_2+OH reaction into the model results in up to 30% decrease in the CH_3O_2 radical concentration while the HO_2 concentration increased by up to 15%. Production and destruction of O_3 are also influenced by these changes, and the model indicates that taking into account the reaction between CH_3O_2 and OH leads to a 6% decrease of O_3.

TOC Graph

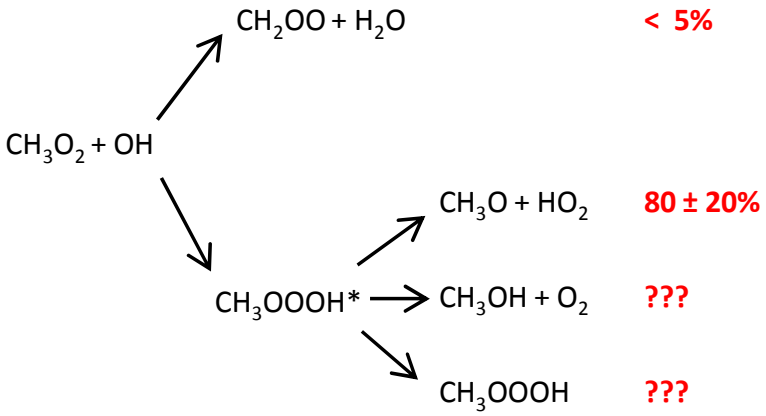

Introduction

Peroxy radicals, RO_2, are key species in atmospheric and low temperature combustion chemistry. They are reactive intermediates formed during the oxidation of all hydrocarbons. In the atmosphere, their subsequent fate depends on the concentration of NOx. In polluted environments at high NOx they will rapidly be removed by reaction with NO to form NO_2. Subsequent photolysis of NO_2 will lead to an increase in O_3 concentration. With decreasing NO concentration, other reaction pathways become competitive for RO_2: the self- and cross-reactions with HO_2 or other RO_2 radicals, leading mostly to stable products[1]. Recently, a new reaction pathway has been suggested as a competitive fate for RO_2 in clean environments, namely the reaction of RO_2 with OH radicals[2,3]. Archibald *et al.*[2] have investigated in a modeling study the impact of including the reaction between RO_2 and OH on the composition of the Marine Boundary Layer (MBL). Different scenarios were run using the BAMBO model , based on the Master Chemical Mechanism, MCM[4]. Different rate constants and reaction paths were considered for RO_2 up to C_4, and for the simplest one, CH_3O_2, leading to the following products:

$$OH + CH_3O_2 \rightarrow CH_2OO + H_2O \qquad (R1a)$$

$$OH + CH_3O_2 \rightarrow CH_3O + HO_2 \qquad (R1b)$$

$$OH + CH_3O_2 \rightarrow CH_3OH + O_2 \qquad (R1c)$$

Archibald *et al*. found for all possible reaction channels only a small, negligible effect on the mixing ratios of O_3, NO_x, OH and other trace gas species in the marine boundary layer. However, a substantial increase in the mixing ratios of HCOOH was predicted (from 0.16 ppt in the base case, i.e. absence of (R1), to 25.5 ppt at the scenario with the largest rate constant), if the reaction pathway were the formation of the Criegee radical (R1a). A strong increase in the mixing ratio of CH_3OH (from 37 ppt in the base case, i.e. absence of (R1), to 294 ppt at the largest rate constant scenario) resulted if the major pathway were (R1c): the impact on stable species was the smallest if (R1b) was the major path. *Ab initio* calculations[5,6] predict pathway (R1b) to be the major reaction, with possible minor contributions of (R1c). Very recently, Müller *et al.*[6] have implemented the title reaction into a global atmospheric chemistry model and have shown, that a yield of around 18% for (R1c) could explain a large missing source of methanol over remote oceans. It seems therefore important to determine experimentally the product distribution of (R1).

The rate constant has been measured recently for the first time for the two simplest peroxy radicals[7-10]

$$CH_3O_2 + OH \rightarrow \text{ products} \qquad (R1)$$

$$C_2H_5O_2 + OH \rightarrow \text{products} \qquad (R2)$$

Large rate constants $k_1 = (2.8\pm1.4)\times10^{-10}$ cm^3s^{-1} and $k_2 = (1.2\pm0.3)\times10^{-10}$ cm^3s^{-1} have been measured by our group for CH_3O_2[7] and $C_2H_5O_2$[8], respectively, although k_1 has very recently been revised by our group to a lower value[9]: $k_1=(1.60\pm0.4)\times10^{-10}$ cm^3s^{-1}. The rate constant k_1 has also recently been determined by Yan *et al.*[10] with an even lower value of $k_1=(0.84\pm0.17)\times10^{-10}$ cm^3s^{-1} deduced from

fitting UV-absorption signals to a complex mechanism. Because these reactions are fast, they can become competitive with other reaction paths for RO_2 radicals. Fittschen *et al.*[3] have integrated (R1) into a detailed box model utilizing the MCM [11] and have determined its importance as a sink for CH_3O_2 radicals in remote marine environments. Running the model using conditions found in the remote tropical marine boundary layer during a field campaign at Cape Verde in 2007[11] have shown that using the initially reported rate constant from Bossolasco *et al.*[7] results in up to 30% of all CH_3O_2 radicals being removed through (R1)[3,6]. The revised rate constant of Assaf *et al.*[9] will decrease the importance of (R1); yet, this reaction is still a substantial sink for CH_3O_2. However, in order to evaluate the impact of this reaction on the composition of the atmosphere it is essential to identify the reaction products. In the current paper we present experiments for the determination of the yields of two possible products: HO_2 radicals from path (R1b) and the Criegee intermediate from path (R1a). The results of these experiments have been implemented into a box model utilizing the MCM, and the impact on the composition of the remote atmosphere has been determined.

Experimental section

HO_2 yield by cw-cavity ring down spectroscopy (CRDS)

An improved version of a well-described set-up[12-15], installed at the University of Lille, has been used to quantify simultaneously OH, HO_2 and CH_3O_2 radicals by two cavity ring down spectroscopy (cw-CRDS) absorption paths, crossing in a slow flow reactor and at a small angle to an Excimer laser photolysis beam. One cavity was equipped with mirrors optimized for a detection of CH_3O_2 radicals at 7489.16 cm^{-1}, the other beam path was used for a sequential detection of HO_2 radicals[16] at 6638.205 cm^{-1} and OH radicals[17] at 7028.831 cm^{-1}. The sequential detection of both species, OH and HO_2, is fast and simple, as the mirrors cover the wavelength region for both species, OH and HO_2. The entire beam path is fibered coupled and changing the wavelength can be accomplished in less than one minute by switching the fiber connectors of the distributed feedback (DFB) lasers without re-alignment of the cavity. Typical kinetic decays are obtained by acquiring ring-down events over several photolysis pulses (20 to 50), and ring-down times τ are converted to absorbance α by the following equation:

$$\alpha_t = [A]_t \times \sigma = \frac{R_L}{c}\left(\frac{1}{\tau_t} - \frac{1}{\tau_0}\right) \qquad \text{[Eq. 1]}$$

The quantity τ_0 and τ_t are the ring-down times in the presence and absence of the absorbing species, in our case before and after the photolysis pulse, respectively; σ is the absorption cross section of the absorbing species; R_L is the ratio between cavity length (79 cm) and absorption length (in our case the

overlap of photolysis laser and near IR laser which is 37.7 cm); *c* is the speed of light. For more details on the synchronization and acquisition see Parker *et al*.[14].

Radicals have been generated from the 248 nm photolysis of XeF_2, which is a solid and easy to handle. Mixtures have been prepared by introducing a few crystals (0.3-0.5 g) into a home-made Teflon bag, which was then filled with around 50 l helium. Evaporation of the crystals led to XeF_2 concentrations of around 1Torr, well below its vapor pressure of (≈5 Torr[18]). Stable flows of this mixture were introduced into the photolysis reactor through a Teflon needle valve: the flow rate was determined through measurement of pressure increase into a known volume. More details on the use of XeF_2 as a photolytic source of F-atom can be found in a recent paper[9].

A total of four experiments has been carried out, all at a total pressure of 50 Torr and 295K. The concentrations are summarized in **Table 1**.

Table 1: Initial concentrations of stable species and maximum radical concentrations from cw-CRDS measurements

O_2 / 10^{18} cm^{-3}	He / 10^{17} cm^{-3}	CH_4 / 10^{15} cm^{-3}	[a]XeF_2 / 10^{14} cm^{-3}	[b]CH_3O_2 / 10^{12} cm^{-3}	[b]OH / 10^{12} cm^{-3}	[b]$HO_{2,max}$ / 10^{12} cm^{-3}
1.30	3.0	1.00	1.94	4.3	0.45	0.58
1.11	5.0	0.82	3.72	8.2	1.7	2.2
1.06	5.5	0.86	4.17	8.9	1.9	2.4
0.86	7.6	0.66	6.04	12.1	4.8	5.2

[a]: estimated from weighted XeF_2 in Teflon bag, [b]: as obtained from cw-CRDS measurements using the absorption cross sections given below

Broadband cavity-enhanced UV spectroscopy

The reaction of OH with CH_3O_2 was also investigated by time-resolved broadband cavity-enhanced UV spectroscopy to test for the possibility of production of formaldehyde oxide, CH_2OO. The experimental apparatus, which was developed at Sandia National Lab, has been described in detail previously[19,20], and only a brief account is given here. The continuous-wave broadband optical buildup cavity was configured to simultaneously probe the spectral range λ = 300 – 450 nm with average effective path length of ~40 m and spectral resolution of 1.5 nm. The optical cavity was integrated into a gas-phase flow reactor with independent control over the experimental temperature, pressure, and sample mixture composition. All experiments were performed at T = 293 K and total P = 30 Torr, and transient UV spectra were recorded with time resolution of 30 μs.

Results and discussion

This section is divided into three sections: details on the determination of HO_2 yield, obtained by cw-CRDS in Lille, are given in the first part; the determination of an upper limit for the yield of Criegee intermediate by UV absorption spectroscopy, obtained at Sandia National Lab, is given in the second part; the implementation in the MCM and the impact of the new findings onto the composition of the troposphere are presented in the third part.

The yield of HO_2 radicals as products of the reaction CH_3O_2 + OH

We have employed a set-up combining two cw-CRDS paths within a laser photolysis reactor to directly quantify the yield of HO_2 radicals, ϕ_{1b}. For this purpose, the reaction has been initiated by the concurrent photolytic production of CH_3O_2 and OH radicals through the following reaction sequence:

$$XeF_2 + h\nu_{248nm} \rightarrow Xe + 2\,F \quad \text{(R3)}$$

$$F + CH_4 \rightarrow HF + CH_3 \quad \text{(R4)}$$

$$CH_3 + O_2 + M \rightarrow CH_3O_2 + M \quad \text{(R5)}$$

$$F + H_2O \rightarrow HF + OH \quad \text{(R6)}$$

The ratio between the initial concentrations of CH_3 and OH radicals is given by the ratio of the rates of (R4) to (R6), ie. the products of the rate constant and the corresponding precursor concentration (CH_4 or H_2O). The subsequent reaction (R5) is under our conditions (≈30 Torr O_2) very fast ($k'_5 \approx 1.3\times10^5$ cm^3s^{-1}) and it can be considered that all CH_3 radicals are converted to CH_3O_2. CH_3O_2 radicals have been quantified on one absorption path, while HO_2 and OH radicals have been quantified sequentially on the second path.

The line strength of a ground state $X^2\Pi_{1/2}$ transition of OH radicals in the near infrared region at 7028.831 cm^{-1} has been very recently determined by Assaf and Fittschen[17] to be $S = 4.07\times10^{-21}$ cm, with a peak absorption cross section at 50 Torr helium of $\sigma_{OH,\ 50\ Torr\ He} = (1.54\pm0.1)\times10^{-19}$ cm^2. The current work has been carried out in the presence of high O_2 concentrations (25 to 40 Torr, the complement to 50 Torr being mostly He from the XeF_2 flow), and therefore the peak absorption cross section will be somewhat lower due to increased pressure broadening of O_2 compared to He. Unfortunately, the O_2 broadening coefficient γ_{O_2} for the line used in this work is currently not known and has been estimated. In the Hitran data base[21] one finds the broadening coefficient in air to be γ_{air} = 0.095 $cm^{-1}atm^{-1}$. Taking this value, i.e. considering an identical broadening efficiency for O_2 and N_2, one can calculate from the line strength[17] and considering a Voigt profile $\sigma_{OH,\ 50\ Torr\ air} = 1.16\times10^{-19}$ cm^2. Taking into account the varying He/O_2 ratios, the peak absorption cross section for the different experiments vary between $(1.23 - 1.34)\times10^{-19}$ cm^2. The average value of $\sigma_{OH} = 1.27\times10^{-19}$ cm^2 of has

been used in [Eq. 1] to convert α_{OH} into [OH]. An uncertainty of 20% is estimated for this absorption cross section.

The absorption cross section for CH_3O_2 has been taken from Farago *et al.*[22]. For HO_2 it has been taken from Thiébaud *et al.*[23]: this line has an absorption cross section nearly two times higher than surrounding lines and is probably the convolution of two nearly perfectly overlapping transition. As a result the pressure broadening in Helium[24] or in O_2[25] is very small. The uncertainty of σ_{HO_2} is estimated to be less than 10%.

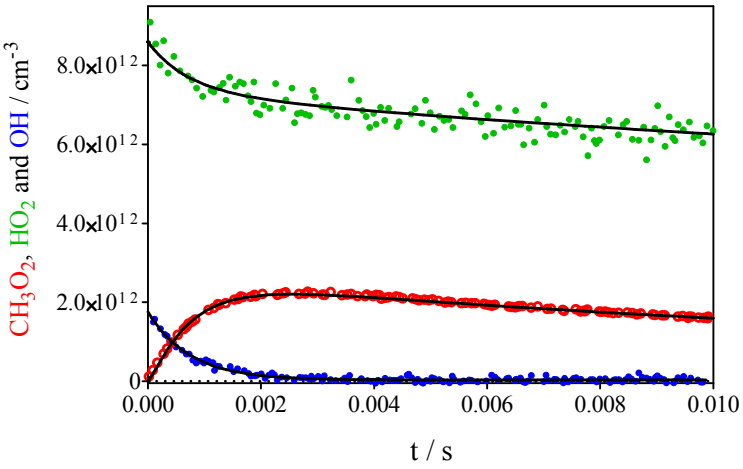

Figure 1: Absolute concentrations of CH_3O_2 (green symbols), HO_2 (red symbols) and OH (blue symbols) following the photolysis of $[XeF_2] = 3.7\times10^{14}$ cm^{-3} in the presence of $[CH_4] = 6.8\times10^{14}$ cm^{-3}, $[H_2O] = 7\times10^{14}$ cm^{-3}, $[He] = 5.0\times10^{17}$ cm^{-3} and $[O_2] = 1.1\times10^{18}$ cm^{-3}. Absorption cross sections of $\sigma_{CH_3O_2} = 3.33\times10^{-20}$cm^2, $\sigma_{HO_2}=2.72\times10^{-19}$ cm^2 and $\sigma_{OH}=1.27\times10^{-19}$ cm^2 have been used for conversion of absorbances α for the three species. The black lines represent adjustment to the model in **Table 2**.

Figure 1 shows a typical experiment at 50 Torr total pressure, using the following concentrations: $[XeF_2] = 3.7\times10^{14}$ cm^{-3}, $[CH_4] = 6.8\times10^{14}$ cm^{-3}, $[H_2O] = 7\times10^{14}$ cm^{-3} , $[He] = 5.0\times10^{17}$ cm^{-3} and $[O_2] = 1.1\times10^{18}$ cm^{-3}. The concentration time profiles of all three species are presented. It can be seen that the initial fast decay in CH_3O_2 concentration is on the same order of magnitude as the decay of the initial OH concentration. It can also be seen that the maximum HO_2 concentration is slightly higher than the initial OH concentration, suggesting a high yield of HO_2 radicals produced in (R1). In order to determine the HO_2 yield, ϕ_{HO_2}, the concentration time profiles have been adjusted to a simple model, with the reactions and rate constants shown in **Table 2**.

Table 2: Reaction mechanism used to fit CH_3O_2, OH and HO_2 concentration time profiles

No.	Reaction	k / cm^3 s^{-1}	Reference
1a	$CH_3O_2 + OH \rightarrow CH_2OO + H_2O$	0	This work and[9]
1b	$\rightarrow HO_2 + CH_3O$	$(1.25\pm0.3)\times10^{-10}$	

1c	→ products *	$(0.35\pm0.3) \times 10^{-10}$	
5	$CH_3 + O_2$ (+M) → CH_3O_2 (+M)	$1.4 \times 10^{-13,**}$	*26,27*
7	$CH_3O + O_2 \rightarrow CH_2O + HO_2$	1.92×10^{-15}	*28*
8a	$2\ CH_3O_2 \rightarrow 2\ CH_3O + O_2$	1.3×10^{-13}	*28*
8b	$2\ CH_3O_2 \rightarrow$ products	2.2×10^{-13}	*28*
9	$CH_3O_2 + HO_2 \rightarrow$ products	5.2×10^{-12}	*28*
10	$2\ HO_2 \rightarrow$ product	1.7×10^{-12}	*29*
11	$OH + HO_2 \rightarrow$ product	1.0×10^{-10}	*29,17*
12	$HO_2 \rightarrow$ diffusion	$8 - 22\ s^{-1}$	This work

*no information about the products can be obtained from the current experiments **Rate constant in 50 Torr helium

Four experiments have been carried out with changing XeF_2 concentrations, leading to initial total radical concentrations between $5 - 17 \times 10^{12}$ cm^{-3} and with ratios of CH_3O_2 / OH between 3 and 12 (see Table 1). All four experiments can be very well reproduced with the mechanism and rate constants from **Table 2**, i.e. ϕ_{HO_2}=0.8.

The uncertainty of the rate constant of (R7), leading to formation of a second HO_2 radical, is given[28] with ±50%. However, the O_2 concentration in our experiments is high, so that this reaction is not the rate limiting step and an uncertainty of k_7 has only a very minor impact on the HO_2 profile. Also, the reactions of CH_3O with OH or HO_2 are probably not important, even though their rate constants are not well known: taking an estimated rate constant [30] of 3×10^{-11} cm^3 s^{-1} for the reaction with OH, even under the most unfavorable conditions (high radical and low O_2 concentration), only 1% of the initial OH radicals would react with CH_3O. The influence of (R8) and (R9) are very limited at short reaction times, and therefore any uncertainty of k_8 and k_9 would have a negligible influence on the retrieval of ϕ_{HO_2}. Equally, the uncertainty of k_{11} has only a limited influence on ϕ_{HO_2}: while the reaction itself consumes around 10% of the initial OH radicals at the experiment with the highest, initial radical concentration, the estimated error of 15% on k_{11} would lead to a change of less than 3% in ϕ_{HO_2}.

The major uncertainty of the retrieved value of ϕ_{HO_2} comes from uncertainties in the absorption cross sections used in [Eq. 1] to convert the absorbance α of OH and HO_2 radicals into absolute concentrations. While the absorption cross section of HO_2 radicals is well determined[24,31,32] and the uncertainty is estimated to be less than 10%, σ_{OH} has only been determined once[17]. Additionally, the value used in this work needs to take into account the increased pressure broadening by the high O_2 concentrations. Therefore, the uncertainty on the OH absorption cross section is estimated to be 20%.

The impact of this uncertainty on the retrieved ϕ_{HO_2} is illustrated in the left graph of **Figure 2**, using the same experiment as shown in **Figure 1** (zoomed on OH and HO_2 only, the CH_3O_2 profile is not shown). The black lines show the model using $\sigma_{OH}=1.27\times10^{-19}$ cm^2, while for the blue and red lines the absorption cross section for OH has been varied by 20%. Using the lower limiting value of σ_{OH} in [Eq. 1] leads to higher OH concentration (red dashed line: the corresponding experimental data points, i.e. the black circles multiplied by 1.2, are not plotted in **Figure 2** for clarity). The model allows a good reproduction of OH and HO_2 profiles, but in order to make up for the higher initial OH concentration, the yield of HO_2 radicals must be decreased (ϕ_{HO_2} = 0.67). The higher value for σ_{OH} (dashed blue line), leading to lower OH concentrations, also allows a satisfactory reproduction of the HO_2 profile, now with ϕ_{HO_2} = 0.96.

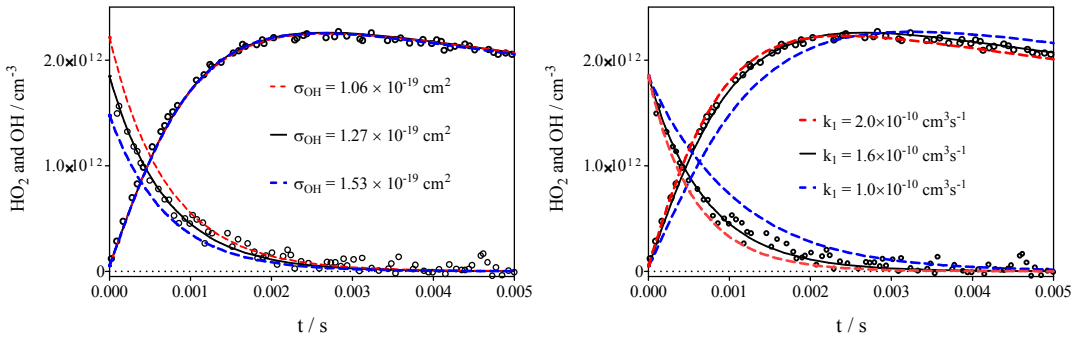

Figure 2: Concentration time profiles for OH (decaying profile) and HO_2 (rising profile) from the experiment shown in **Figure 1**, reproduced with the model utilizing the chemical mechanism from **Table 2**. Left graph: Influence of a 20% uncertainty of σ_{OH} on the HO_2 concentration time profile: full black line OH concentrations obtained by using $\sigma_{OH}=1.27\times10^{-19}$ cm^2, red dashed line with σ_{OH} decreased by 20%, blue dashed line with σ_{OH} increased by 20% (the corresponding experimental OH data are not plotted for clarity). ϕ_{HO_2} = 0.67, 0.8 and 0.96 for the red, black and blue lines, respectively. Right graph: Impact of the rate constant k_1 on both profiles: all rate constants as in **Table 2**, only k_1 has been changed.

The right graph of **Figure 2** shows the sensitivity of the experimental data to the rate constant k_1, whereby the total value has been varied between 1 and 2 × 10^{-10} cm^{3}s^{-1}. In order to reproduce the absolute HO_2 concentration, k_{1b} and k_{1c} have been adjusted to (9/1), (12.5/3.5) and (15/5) × 10^{-11} cm^{3}s^{-1} for the blue, black and red curves. The blue line represents the upper limit of the rate constant recently published by Yan *et al.*[10]. A change in k_1 has a strong impact on the predicted HO_2 profile in our experiment. Not only would the rise time of HO_2 slow down with a decrease in k_1, but also the final, maximum HO_2 concentration would decrease. This is because the conversion of OH into HO_2 through (R1) is not only governed by ϕ_{HO_2}, but also by the rate constant k_1: a lower rate constant leads to a lower conversion because competing reactions gain in importance, especially the fast reaction (R11). The black line shows the best fit for both species with $k_1=1.6\times10^{-10}$ cm^{3}s^{-1}. The dotted red lines correspond to the model using $k_1=2\times10^{-10}$ cm^{3}s^{-1}: OH and HO_2 profiles are barely reproduced with this

faster rate constant, the retrieved HO_2 yield would be similar with ϕ_{HO_2} = 0.75. A decrease to k_1 = 1×10^{-10} cm^3s^{-1} results in a very poor reproduction the OH and HO_2 profiles: the time evolution is too slow for both species. With this rate constant, ϕ_{HO_2} would rise to ϕ_{HO_2} = 0.9 because other loss reactions, especially (R11), gain in importance.

In conclusion, our determination of the HO_2 yield at a total pressure of 50 Torr O_2 / He shows that HO_2 is the major product with ϕ_{HO_2}= 0.8±0.2.

Determination of an upper limit for the yield of Criegee intermediate CH_2OO

The Criegee intermediate CH_2OO is the product of channel (R1a). Theoretical calculations predict this pathway to be of minor importance[5,6], and recent experiments of Yan et al.[10] using UV absorption spectroscopy have determined an upper limit of 5% on channel (R1b). Experiments have been carried out at Sandia National Laboratory. XeF_2 was not available to initiate the reaction by the same reaction sequence as in Lille, also the absorption cross section would be even lower at the used wavelength. Therefore, the reaction sequence was initiated by 266-nm photolysis of acetone vapor in He bath gas in the presence of 2.5 Torr (8.25×10^{16} cm^{-3}) of O_2. The reaction sequence begins with concurrent photolytic production of methyl and acetyl radicals (at an estimated ratio of ~1.5:1) and subsequent rapid reaction of these radicals with excess O_2 forms CH_3O_2 and OH[33-35]; within less than 1 ms, as summarized below:

$CH_3COCH_3 + h\nu \rightarrow CO + 2\ CH_3$	~20%	(R 13a)
$\rightarrow CH_3CO + CH_3$	~80%	(R 13b)
$CH_3 + O_2\ (+ M) \rightarrow CH_3O_2\ (+ M)$	~100%	(R 5)
$CH_3CO + O_2 \rightarrow OH +$ co-products	10 - 50%	(R 14)

The yield of OH radicals in (R14) is pressure dependant and still controversially discussed: Carr et al.[34] for example report a yield of $\phi_{OH} \approx 0.5$ for (R14) at 50 Torr, while recent publications of Papadimitriou et al.[36] and Bouzidi et al.[25] report yield of 0.1 – 0.2 at 20 Torr. Therefore, CH_3O_2 is generated by this system in excess over OH (ratio CH_3O_2 : OH ≈ (3-15) : 1). Two different experimental runs were performed. In the first, the initial molar fraction of acetone was adjusted to produce an estimated $[CH_3O_2] = 4.8\times10^{12}$ cm^{-3} and a lower limit for $[OH] \geq 3.2\times10^{11}$ cm^{-3}; in the second, the acetone concentration was increased to form $[CH_3O_2] = 8.9\times10^{12}$ cm^{-3} and $[OH] \geq 6\times10^{11}$ cm^{-3}.

The resulting transient spectra, averaged over kinetic times 0 – 5 ms, are presented in **Figure 3**. The spectra reveal a single broad absorption feature with maximum intensity at the low-wavelength edge

of the accessible experimental range, 300 nm, which most likely arises solely from the methyl peroxy radical. Simulations (also shown in **Figure 3**) of the predicted transient signal using the reported absorption cross-section of CH_3O_2 at 300 nm[37], $\sigma = 3.3\times10^{-19}$ cm^2, are in qualitative agreement with the observed spectra, which confirms our expectations of methyl peroxy radical concentration formed by reactions (R5) and (R13). The time evolution of the CH_3O_2 absorption is included as the inset in **Figure 3**.

Small Criegee intermediates such as formaldehyde oxide and acetaldehyde oxide were recently shown[20,38-40] to have very strong UV absorption bands in the 300 – 400 nm range with peak absorption cross-sections of the B←X transition of $\sim1\times10^{-17}$ cm^2. Thus, UV absorption is a sensitive detection method for Criegee intermediates, and our experiments have a detection limit for CH_2OO below $\sim5\times10^8$ cm^{-3}. Transient absorption due to CH_2OO is expected to decay on the timescale of a few ms, primarily due to the reaction with excess acetone vapor[41], yet we observe essentially no decaying signals in our experiment. The presence of transient CH_3O_2 absorption somewhat obscures our probe spectral region; nonetheless, based on the signal near the peak of CH_2OO spectrum ($\lambda \sim 360$ nm), we can report a realistic upper limit for CH_2OO concentration of $<1\times10^{10}$ cm^{-3} in our experiments. Even if we adopt the most conservative possible approach and assign all of the transient absorption at 360 nm to CH_2OO, the upper limit for its concentration at t=1 ms is still below 2.5×10^{10} cm^{-3}. Being again conservative and using the lower limit for the OH-concentration this leads to an upper limit of $\phi_{1a} < 0.05$. This result is in very good agreement with theoretical calculations, but also with the recent finding of Yan et al.[10], who also determined an upper limit of $\phi_{1a} < 0.05$ for the formation of the Criegee intermediate in (R1).

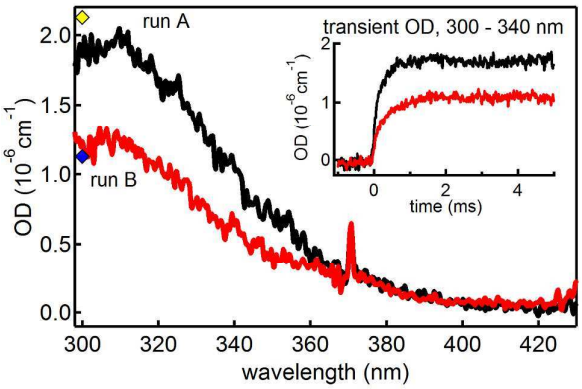

Figure 3: Experimental transient spectra, averaged over the kinetic times 0 – 5 ms following the 248 nm photolysis of acetone in He bath gas in the presence of 2.5 Torr O_2 (total P = 30 Torr). Inset: transient absorption, averaged over probe λ = 300 – 340 nm, as a function of kinetic time. Red and black spectra and kinetic traces are from run A ($[CH_3O_2] = 8.9\times10^{12}$ cm^{-3} and $[OH] = 3\times10^{12}$ cm^{-3}) and B ($[CH_3O_2] = 4.8\times10^{12}$ cm^{-3} and $[OH] = 1.6\times10^{12}$ cm^{-3}), respectively. Blue and yellow diamonds show the simulated transient absorption at 300 nm for run A and B, respectively, assuming that only CH_3O_2 contributes to the signal.

Modeling and Atmospheric Implication

A box model constrained to the Master Chemical Mechanism v3.2 has been run to test the atmospheric significance of HO_2 production from the reaction of OH with CH_3O_2 under clean, low NO_x conditions. The model was constrained with gas-phase composition field data (including the concentrations of the halogen oxides IO and BrO), photolysis rates and meteorological parameters taken during the RHaMBLe project that took place in 2007[42] at the Cape Verde Atmospheric Observatory (CVAO) which is situated on the island of Sao Vicente in the tropical Atlantic Ocean (23.96° S, 46.39° W). This model has been described previously and was used to calculate OH and HO_2 concentrations for comparison with those measured at the CVAO[11]. Inclusion of reaction (R1b) in the model has a substantial impact on the predicted CH_3O_2 levels, decreasing the concentration of CH_3O_2 by ~30% during the afternoon (**Figure 4**). Taking into account the HO_2 (and CH_3O) production from (R1b) reported here, the model predicts approximately 20% more HO_2 at CVAO (**Figure 4**). This increase in modeled HO_2 further enhances the destruction of CH_3O_2 (alongside the enhanced destruction due to the reaction with OH) by increasing the loss of CH_3O_2 via reaction with HO_2 (by 15%) which is the dominant CH_3O_2 sink, accounting for 50% of the total CH_3O_2 destruction in this environment.

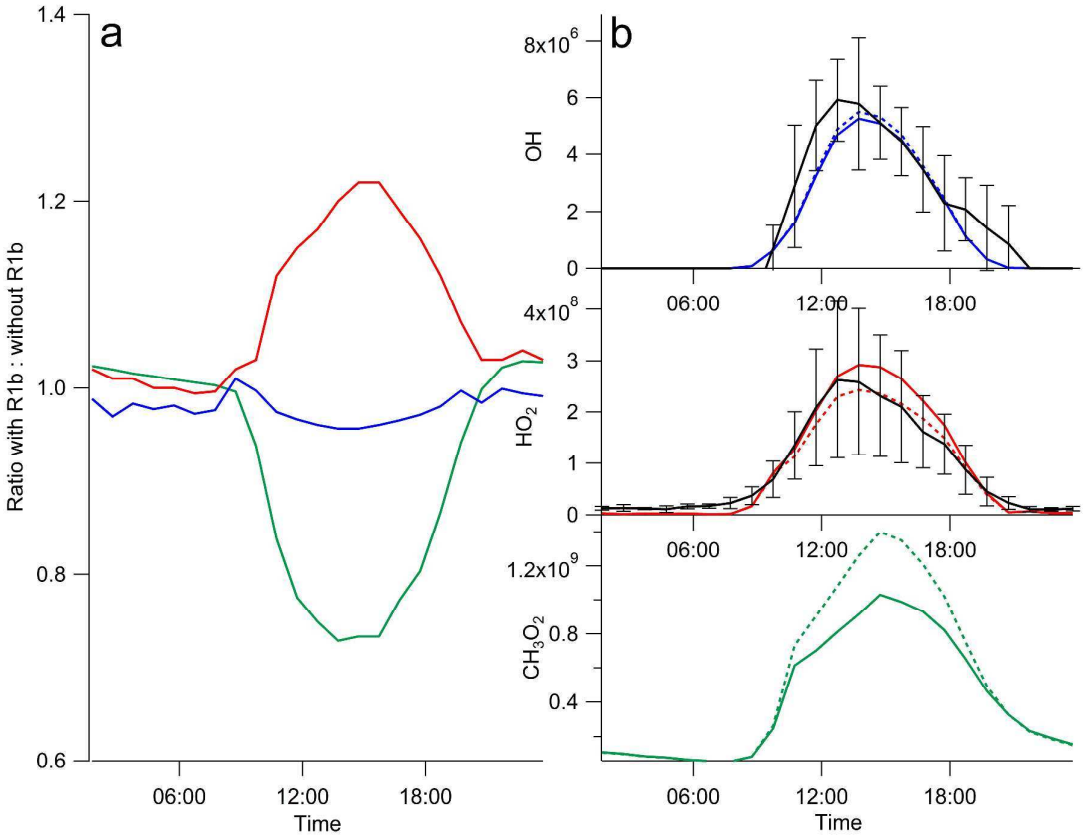

Figure 4a: Diurnal ratios of modelled radical concentrations with reaction (R1b) included: without reaction (R1b) included in the model simulations. **b:** Diurnal concentrations of modelled OH (blue), HO_2 (red) and CH_3O_2 (green) (with R1b – solid coloured lines, without R1b – dashed coloured lines) compared with measured OH and HO_2 (black lines). Errors bars represent the 1σ day-to-day variability in the averaged data.

Tropospheric ozone is an important greenhouse gas and in remote oceanic regions, integrating (R1b) into a model impacts also on its formation and destruction paths. At conditions such as found at the CVAO, ozone production via reaction of peroxy radicals with NO is small, and ozone is typically destroyed during the day via deposition and photochemical reactions (**Table 3**). HO_2 accounts for 9% of the daily ozone destruction cycle observed at CVAO and, as the reaction of CH_3O_2 with O_3 is significantly slower than the reaction of HO_2 with O_3, overlooking an additional source of HO_2 from reaction (R1b) may influence model estimates of ozone destruction (dO_3). The reaction of HO_2 with ozone proceeds ~ 17% faster when (R1b) is included; the reactions of HO_2 with IO and BrO are also enhanced by ~ 18% and this serves to increase dO_3 further. Considering all the net ozone destroying reactions (**Table 3**), it is estimated that (R1b) enhances dO_3 by ~4%. Reaction (R1b), also serves to modify ozone production (pO_3) by a reduction in the rate of CH_3O_2+NO and an enhancement in the rate of HO_2+NO reactions. Overall pO_3 is predicted to decrease modestly (by ~75 pptv d^{-1}) when (R1b) is considered and so taking both the changes in pO_3 and dO_3 into account, this study suggests that tropospheric ozone in remote regions will be over-estimated by ~6% by models which do not consider the reaction of CH_3O_2 with OH. Remote oceanic regions cover approximately two thirds of the Earth's surface and so omission of the reaction of CH_3O_2 with OH yielding HO_2 may lead to significant over-predictions in tropospheric ozone on a global scale.

Table 3: Percentage contribution of the rate limiting O_3 destruction steps with and without (R1b) included in the model simulation

O_3 destruction rate determining step	% Contribution to O_3 destruction without (R1b)	% Contribution to O_3 destruction with (R1b)
$O^1D + H_2O$	62.8	60.2
$OH + O_3$	5.8	5.3
$HO_2 + O_3$	8.5	9.5
$BrO + HO_2$	5.1	5.7
BrO + NO	1.1	1.1
BrO + BrO	0.2	0.2
BrO + IO	2.3	2.2
$IO + HO_2$	11.7	13.2
IO + NO	0.8	0.7
IO + IO	2.0	2.0

The concentration of methanol is generally underpredicted by global models compared to the measured CH_3OH concentration. In the recent work of Müller *et al.*[6] it was proposed that a significant yield of CH_3OH in (R1) could help to explain this discrepancy. The best estimate from their theoretical calculations predict yields for CH_3OH and for the stabilized CH_3OOOH between 0.05 and 0.1, but each with a wide error margin of a factor ~3.5. This is in very perfect agreement with the measurements presented in this word. However, in order to best reproduce measured CH_3OH concentrations, a CH_3OH yield of 18%, together with a yield of 21% for stabilization of the initially formed trioxide, CH_3OOOH, would be needed. This scenario leaves a yield of 61% for HO_2 formation through channel (R1b). However, Müller *et al*. used for their model the excessively high rate constant of Bossolasco *et al.*[7], and hence their study overstates the overall importance of (R1). As a result the CH_3OH yield would need to be increased further (leading consequently to an even lower value for the HO_2 yield) in order to bring into agreement the CH_3OH predictions with measurements. While a yield of 61% HO_2 would be within the error limit of the current work, an even higher value is not in agreement with the above presented measurements. However, it has to be noted that the current measurements for the HO_2 yields have been carried out at low pressure (50 Torr helium / O_2) and that the product distribution might change with pressure. Therefore, product distributions should be determined at higher pressures in order to find out if the title reaction could be a significant source of CH_3OH in the remote troposphere. The present set-up is not very suitable for this task, because the absorption lines of OH and HO_2 suffer from broadening, making their detection at higher pressure less sensitive. Also the uncertainty of the derived yield would increase, if the appropriate broadening coefficients are not well known. The better way would be the direct detection of CH_3OH, but unfortunately the cw-CRDS set-up is not sensitive to this species.

Acknowledgements

This project was supported by the French ANR agency under contract No. ANR-11-LabEx-0005-01 CaPPA (Chemical and Physical Properties of the Atmosphere). Development of the time-resolved broadband cavity-enhanced UV spectrometer was supported by the Laboratory-Directed Research and Development (LDRD) program at Sandia National Laboratories. Sandia is a multi-mission laboratory operated by Sandia Corporation, a Lockheed Martin Company, for the National Nuclear Security Administration under contract DE-AC04-94-AL85000. DEH and LKW are grateful to the Natural Environment Research Council for funding.

References

(1) Tyndall, G. S.; Cox, R. A.; Granier, C.; Lesclaux, R.; Moortgat, G. K.; Pilling, M. J.; Ravishankara, A. R.; Wallington, T. J., Atmospheric Chemistry of Small Organic Peroxy Radicals, *J. Geophys. Res.* **2001**, *106*, 12157-12182

(2) Archibald, A. T.; Petit, A. S.; Percival, C. J.; Harvey, J. N.; Shallcross, D. E., On the Importance of the Reaction between OH and RO_2 Radicals, *Atmos. Sci. Lett.* **2009**, *10*, 102-108

(3) Fittschen, C.; Whalley, L. K.; Heard, D. E., The Reaction of CH_3O_2 Radicals with OH Radicals: A Neglected Sink for CH_3O_2 in the Remote Atmosphere, *Environ. Sci. Technol.* **2014**, *118*, 7700–7701

(4) Saunders, S. M.; Jenkin, M. E.; Derwent, R. G.; Pilling, M. J., Protocol for the Development of the Master Chemical Mechanism, MCM v3 (Part A): Tropospheric Degradation of Non-Aromatic Volatile Organic Compounds, *Atmos. Chem. Phys.* **2003**, *3*, 161-180

(5) Bian, H.; Zhang, S.; Zhang, H., Theoretical Study on the Atmospheric Reaction of CH_3O_2 with OH, *Int. J. Quantum Chem* **2015**, *115*, 1181-1186

(6) Müller, J.-F.; Liu, Z.; Nguyen, V. S.; Stavrakou, T.; Harvey, J. N.; Peeters, J., The Reaction of Methyl Peroxy and Hydroxyl Radicals as a Major Source of Atmospheric Methanol, *Nature Communications* **2016**, *7*, 13213

(7) Bossolasco, A.; Faragó, E. P.; Schoemaecker, C.; Fittschen, C., Rate Constant of the Reaction between CH_3O_2 and OH Radicals, *Chem. Phys. Lett.* **2014**, *593*, 7-13

(8) Faragó, E. P.; Schoemaecker, C.; Viskolcz, B.; Fittschen, C., Experimental Determination of the Rate Constant of the Reaction between $C_2H_5O_2$ and OH Radicals, *Chem. Phys. Lett.* **2015**, *619*, 196-200

(9) Assaf, E.; Song, B.; Tomas, A.; Schoemaecker, C.; Fittschen, C., Rate Constant of the Reaction between CH_3O_2 Radicals and OH Radicals revisited, *J. Phys. Chem. A* **2016**, *120*, 8923-8932

(10) Yan, C.; Kocevska, S.; Krasnoperov, L. N., Kinetics of the Reaction of CH_3O_2 Radicals With OH Studied Over the 292 – 526 K Temperature Range, *J. Phys. Chem. A* **2016**, *120*, 6111–6121

(11) Whalley, L. K.; Furneaux, K. L.; Goddard, A.; Lee, J. D.; Mahajan, A.; Oetjen, H.; Read, K. A.; Kaaden, N.; Carpenter, L. J.; Lewis, A. C.; Plane, J. M. C.; Saltzman, E. S.; Wiedensohler, A.; Heard, D. E., The Chemistry of OH and HO_2 Radicals in the Boundary Layer over the Tropical Atlantic Ocean, *Atmos. Chem. Phys.* **2010**, *10*, 1555-1576

(12) Thiebaud, J.; Fittschen, C., Near Infrared cw-CRDS Coupled to Laser Photolysis: Spectroscopy and Kinetics of the HO_2 Radical, *Appl. Phys. B* **2006**, *85*, 383-389

(13) Parker, A.; Jain, C.; Schoemaecker, C.; Fittschen, C., Kinetics of the Reaction of OH Radicals with CH_3OH and CD_3OD Studied by Laser Photolysis Coupled to High Repetition Rate Laser Induced Fluorescence, *React. Kinet. Catal. Lett.* **2009**, *96*, 291-297

(14) Parker, A.; Jain, C.; Schoemaecker, C.; Szriftgiser, P.; Votava, O.; Fittschen, C., Simultaneous, Time-Resolved Measurements of OH and HO_2 Radicals by Coupling of High Repetition Rate LIF and cw-CRDS Techniques to a Laser Photolysis Reactor and its Application to the Photolysis of H_2O_2 *Appl. Phys. B* **2011**, *103*, 725-733

(15) Votava, O.; Masat, M.; Parker, A. E.; Jain, C.; Fittschen, C., Microcontroller Based Resonance Tracking unit for Time Resolved Continuous wave Cavity-Ringdown Spectroscopy Measurements, *Rev. Sci. Instrum.* **2012**, *83*, 043110

(16) Thiebaud, J.; Crunaire, S.; Fittschen, C., Measurement of Line Strengths in the $2\nu^1$ Band of the HO_2 Radical using Laser Photolysis / Continous wave Cavity Ring Down Spectroscopy (cw-CRDS), *J. Phys. Chem. A* **2007**, *111*, 6959-6966

(17) Assaf, E.; Fittschen, C., Cross Section of OH Radical Overtone Transition near 7028 cm^{-1} and Measurement of the Rate Constant of the Reaction of OH with HO_2 Radicals, *J. Phys. Chem. A* **2016**, *120*, 7051-7059
(18) Tellinghuisen, P. C.; Tellinghuisen, J.; Coxon, J. A.; Velazco, J. E.; Setser, D. W., Spectroscopic Studies of Diatomic Noble Gas Halides. IV. Vibrational and Rotational Constants for the X, B, and D States of XeF, *J. Chem. Phys.* **1978**, *68*, 5187-5198
(19) Sheps, L.; Chandler, D. W., Time-resolved broadband cavity-enhanced absorption spectrometry for chemical kinetics; ;,, *Sandia National Laboratories: Livermore, CA,* **2013**, SAND2013-2664
(20) Sheps, L.; Scully, A. M.; Au, K., UV absorption probing of the conformer-dependent reactivity of a Criegee intermediate CH3CHOO, *PCCP* **2014**, *16*, 26701-26706
(21) Rothman, L. S.; Gordon, I. E.; Babikov, Y.; Barbe, A.; Chris Benner, D.; Bernath, P. F.; Birk, M.; Bizzocchi, L.; Boudon, V.; Brown, L. R.; Campargue, A.; Chance, K.; Cohen, E. A.; Coudert, L. H.; Devi, V. M.; Drouin, B. J.; Fayt, A.; Flaud, J. M.; Gamache, R. R.; Harrison, J. J.; Hartmann, J. M.; Hill, C.; Hodges, J. T.; Jacquemart, D.; Jolly, A.; Lamouroux, J.; Le Roy, R. J.; Li, G.; Long, D. A.; Lyulin, O. M.; Mackie, C. J.; Massie, S. T.; Mikhailenko, S.; Müller, H. S. P.; Naumenko, O. V.; Nikitin, A. V.; Orphal, J.; Perevalov, V.; Perrin, A.; Polovtseva, E. R.; Richard, C.; Smith, M. A. H.; Starikova, E.; Sung, K.; Tashkun, S.; Tennyson, J.; Toon, G. C.; Tyuterev, V. G.; Wagner, G., The HITRAN2012 Molecular Spectroscopic Database, *J. Quant. Spectrosc. Radiat. Transfer* **2013**, *130*, 4-50
(22) Faragó, E. P.; Viskolcz, B.; Schoemaecker, C.; Fittschen, C., Absorption Spectrum and Absolute Absorption Cross Sections of CH_3O_2 Radicals and CH_3I Molecules in the Wavelength Range 7473–7497 cm^{-1}, *J. Phys. Chem. A* **2013**, *117*, 12802-12811
(23) Thiebaud, J.; Aluculesei, A.; Fittschen, C., Formation of HO_2 Radicals from the Photodissociation of H_2O_2 at 248 nm, *J. Chem. Phys.* **2007**, *126*, 186101
(24) Morajkar, P.; Bossolasco, A.; Schoemaecker, C.; Fittschen, C., Photolysis of CH_3CHO at 248 nm: Evidence of Triple Fragmentation from Primary Quantum Yield of CH_3 and HCO Radicals and H Atoms, *J. Chem. Phys.* **2014**, *140*, 214308
(25) Bouzidi, H.; Djehiche, M.; Gierczak, T.; Morajkar, P.; Fittschen, C.; Coddeville, P.; Tomas, A., Low-Pressure Photolysis of 2,3-Pentanedione in Air: Quantum Yields and Reaction Mechanism, *J. Phys. Chem. A* **2015**, *119*, 12781-12789
(26) Selzer, E. A.; Bayes, K. D., Pressure Dependence of the Rate of Reaction of Methyl Radicals with Oxygen, *J. Phys. Chem.* **1983**, *87*, 392-394
(27) Fernandes, R. X.; Luther, K.; Troe, J., Falloff Curves for the Reaction $CH_3 + O_2$ (+ M) → CH_3O_2 (+ M) in the Pressure Range 2 - 1000 Bar and the Temperature Range 300 - 700 K, *J. Phys. Chem. A* **2006**, *110*, 4442-4449
(28) Atkinson, R.; Baulch, D. L.; Cox, R. A.; Crowley, J. N.; Hampson, R. F.; Hynes, R. G.; Jenkin, M. E.; M. J. Rossi; Troe, J., Evaluated Kinetic and Photochemical Data for Atmospheric Chemistry: Volume II - Gas Phase Reactions of Organic Species, *Atmos. Chem. Phys.* **2006**, *6*, 3625-4055
(29) Atkinson, R.; Baulch, D. L.; Cox, R. A.; Crowley, J. N.; Hampson, R. F.; Hynes, R. G.; Jenkin, M. E.; Rossi, M. J.; Troe, J., Evaluated Kinetic and Photochemical Data for Atmospheric Chemistry: Volume 1 – Gas Phase Reactions of O_x, HO_x, NO_x, and SO_x, Species, *Atmos. Chem. Phys.* **2004**, *4*, 1461-1738
(30) Tsang, W.; Hampson, R. F., Chemical kinetic data base for combustion chemistry. Part I. Methane and related compounds, *J. Phys. Chem. Ref. Data* **1986**, *15*, 1087
(31) Ibrahim, N.; Thiebaud, J.; Orphal, J.; Fittschen, C., Air-Broadening Coefficients of the HO_2 Radical in the $2\nu_1$ Band Measured Using cw-CRDS, *J. Mol. Spectrosc.* **2007**, *242*, 64-69

(32) Tang, Y.; Tyndall, G. S.; Orlando, J. J., Spectroscopic and Kinetic Properties of HO_2 Radicals and the Enhancement of the HO_2 Self Reaction by CH_3OH and H_2O, *J. Phys. Chem. A* **2010**, *114*, 369-378
(33) Blitz, M. A.; Heard, D. E.; Pilling, M. J., Study of Acetone Photodissociation over the Wavelength Range 248-330 nm: Evidence of a Mechanism Involving Both the Singlet and Triplet Excited States, *J. Phys. Chem. A* **2006**, *110*, 6742-6756
(34) Carr, S. A.; Baeza-Romero, M. T.; Blitz, M. A.; Pilling, M. J.; Heard, D. E.; Seakins, P. W., OH Yields from the $CH_3CO + O_2$ Reaction using an Internal Standard, *Chem. Phys. Lett.* **2007**, *445*, 108-112
(35) Khamaganov, V. G.; Karunanandan, R.; Horowitz, A.; Dillon, T. J.; Crowley, J. N., Photolysis of $CH_3C(O)CH_3$ at 248 and 266 nm: pressure and temperature dependent overall quantum yields., *PCCP* **2009**, *11*, 6173-6181
(36) Papadimitriou, V. C.; Karafas, E. S.; Gierczak, T.; Burkholder, J. B., CH3CO + O2 + M (M = He, N2) Reaction Rate Coefficient Measurements and Implications for the OH Radical Product Yield, *J. Phys. Chem. A* **2015**, *119*, 7481-7497
(37) Maricq, M. M.; Wallington, T. J., Absolute ultraviolet cross sections of methyl and ethyl peroxy radicals, *J. Phys. Chem.* **1992**, *96*, 986-992
(38) Ting, W.-L.; Chen, Y.-H.; Chao, W.; Smith, M. C.; Lin, J. J.-M., The UV absorption spectrum of the simplest Criegee intermediate CH_2OO, *PCCP* **2014**, *16*, 10438-10443
(39) Sheps, L., Absolute Ultraviolet Absorption Spectrum of a Criegee Intermediate CH_2OO, *Journal of Chemical Phyics Letters* **2013**, 4201-4205
(40) Lewis, T. R.; Blitz, M. A.; Heard, D. E.; Seakins, P. W., Direct evidence for a substantive reaction between the Criegee intermediate, CH2OO, and the water vapour dimer, *PCCP* **2015**, *17*, 4859-4863
(41) Taatjes, C. A.; Welz, O.; Eskola, A. J.; Savee, J. D.; Osborn, D. L.; Lee, E. P. F.; Dyke, J. M.; Mok, D. W. K.; Shallcross, D. E.; Percival, C. J., Direct measurement of Criegee intermediate (CH2OO) reactions with acetone, acetaldehyde, and hexafluoroacetone, *PCCP* **2012**, *14*, 10391-10400
(42) Lee, J. D.; McFiggans, G.; Allan, J. D.; Baker, A. R.; Ball, S. M.; Benton, A. K.; Carpenter, L. J.; Commane, R.; Finley, B. D.; Evans, M.; Fuentes, E.; Furneaux, K.; Goddard, A.; Good, N.; Hamilton, J. F.; Heard, D. E.; Herrmann, H.; Hollingsworth, A.; Hopkins, J. R.; Ingham, T.; Irwin, M.; Jones, C. E.; Jones, R. L.; Keene, W. C.; Lawler, M. J.; Lehmann, S.; Lewis, A. C.; Long, M. S.; Mahajan, A.; Methven, J.; Moller, S. J.; Müller, K.; Müller, T.; Niedermeier, N.; O'Doherty, S.; Oetjen, H.; Plane, J. M. C.; Pszenny, A. A. P.; Read, K. A.; Saiz-Lopez, A.; Saltzman, E. S.; Sander, R.; von Glasow, R.; Whalley, L.; Wiedensohler, A.; Young, D., Reactive Halogens in the Marine Boundary Layer (RHaMBLe): the tropical North Atlantic experiments, *Atmos. Chem. Phys.* **2010**, *10*, 1031-1055